Condensin DC spreads linearly and bidirectionally from recruitment sites to create loop-anchored TADs in *C. elegans*

David Sebastian Jimenez[1], Jun Kim[1], Bhavana Ragipani[1], Bo Zhang[2], Lena Annika Street[1], Maxwell Kramer[1], Sarah E Albritton[1], Lara Winterkorn[1], Sevinç Ercan[1&]

[1]Department of Biology, Center for Genomics and Systems Biology, New York University, New York, NY 10003

[2]UCSF 513 Parnassus Ave, HSW, San Francisco CA 94143

[&] Corresponding author
Sevinç Ercan email: sevinc@nyu.edu

key words: condensin, Hi-C, SMC complex, TAD, 3D organization, insulation, loop extrusion, C. elegans, X chromosome, dosage compensation

Abstract

Condensins are molecular motors that compact DNA for chromosome segregation and gene regulation. *In vitro* experiments have begun to elucidate the mechanics of condensin function but how condensin loading and translocation along DNA controls eukaryotic chromosome structure *in vivo* remains poorly understood. To address this question, we took advantage of a specialized condensin, which organizes the 3D conformation of X chromosomes to mediate dosage compensation (DC) in *C. elegans*. Condensin DC is recruited and spreads from a small number of recruitment elements on the X chromosome (*rex*). We found that ectopic insertion of *rex* sites on an autosome leads to bidirectional spreading of the complex over hundreds of kilobases. On the X chromosome, strong *rex* sites contain multiple copies of a 12-bp sequence motif and act as TAD borders. Inserting a strong *rex* and ectopically recruiting the complex on the X chromosome or an autosome creates a loop-anchored TAD. Unlike the CTCF system, which controls TAD formation by cohesin, direction of the 12-bp motif does not control the specificity of loops. In an X;V fusion chromosome, condensin DC linearly spreads into V and increases 3D DNA contacts, but fails to form TADs in the absence of *rex* sites. Finally, we provide *in vivo* evidence for the loop extrusion hypothesis by targeting multiple dCas9-Suntag complexes to an X chromosome repeat region. Consistent with linear translocation along DNA, condensin DC accumulates at the block site. Together, our results support a model whereby strong *rex* sites act as insulation elements through recruitment and bidirectional spreading of condensin DC molecules and form loop-anchored TADs.

Introduction

Eukaryotic chromosome structure is dynamically regulated across the cell cycle. During interphase, genomes are organized within the nucleus [1-4] and go through further compaction for accurate segregation of chromosomes during mitosis and meiosis [5, 6]. Chromosome compaction is mediated in part by DNA looping by a conserved family of protein complexes called the structural maintenance of chromosomes (SMC) [7]. SMC complexes include cohesin and condensin, which are essential for genome organization and segregation [8].

The function of cohesin and condensin in various cellular processes are based on their ability to hold two separate strands of DNA together [9, 10]. These interactions can happen intramolecularly on the same chromosome or intermolecularly bringing different chromosomes in close 3D proximity [11]. Intramolecular activity of condensin and cohesin is important for organizing the 3D contacts between chromosomal sites, forming topologically associated domains (TADs) that act as genetic neighborhoods within which genes are regulated [2, 12-16].

In vitro analysis of condensin and cohesin binding on DNA indicate that they act as ATP dependent molecular motors forming DNA loops by progressively extruding DNA [17-20]. Loop extrusion hypothesis gained *in vivo* support by *in silico* modeling of loop extrusion

activity to explain Hi-C analysis of 3D genome contacts in the presence and absence of condensin and cohesin [5, 21].

The mechanism by which cohesin contributes to formation of TADs is better understood compared to condensin. Cohesin loading and processivity is promoted by the Adherin complex (in yeast Scc2-Scc4, in mammals Nipbl & Mau2) [22, 23] and its unloading is mediated by Wapl [22, 24, 25]. Cohesin translocation on DNA is also controlled by insulator proteins, including the zinc finger transcription factor CTCF, which creates TAD borders [26]. The inhibition of cohesin translocation by CTCF is directional, in which two convergent CTCF binding motifs brought together by DNA looping prevents the passage of cohesin [27].

While *in vitro* and *in silico* experiments suggest similar molecular activities for condensins and cohesins [7], it is less clear how condensin binding and movement on eukaryotic chromosomes are regulated *in vivo*. In yeast, TATA box-binding protein (TBP) and TFIIIC recruit condensin to highly transcribed and tRNA gene promoters [28, 29]. However, since yeast chromosomes support much smaller interaction domains, how condensin binding regulates larger eukaryotic genomes remains unknown. An excellent model to address this gap is a specialized condensin that functions within the X chromosome dosage compensation complex (DCC) in *C. elegans*.

In addition to the canonical condensins I and II, *C. elegans* possess condensin I^{DC} (hereafter condensin DC) that differs from the canonical condensins by a single SMC-4 variant DPY-27 [30]. Condensin DC binds to both X chromosomes in hermaphrodites to repress their transcription by a factor of two, equalizing overall X chromosomal transcripts between XX hermaphrodites and XO males [31-34]. Several features make condensin DC a powerful system to address mechanisms of condensin binding and spreading. First, unlike canonical condensins, the sequence elements important for condensin DC recruitment to the X chromosomes are identified [35-38]. Second, the spreading of the complex can be distinguished from recruitment using X to autosome (X;A) fusion chromosomes, where the complex translocates from the X into the autosome [39]. Third, since the complex only binds to the X chromosomes, autosomes serve as internal controls, allowing sensitive measurement using genomics approaches [40-42].

Condensin DC recruitment to the X chromosomes is mediated by ~60 recruitment elements on the X (*rex* sites) [35-37]. The complex is thought to spread from the *rex* sites, accumulating at enhancers, promoters, and other accessible gene regulatory elements along the chromosome [41]. Deletion of individual *rex* sites reduces DCC binding ~ 1Mb around it, indicating that while each *rex* site contributes to condensin DC binding around it, multiple *rex* sites support robust binding across the ~17 Mb X chromosomes [35].

Hi-C analysis in *C. elegans* embryos indicated that eight strong *rex* sites function as TAD borders [43]. This reflects a subset of approximately 60 *rex* sites and seventeen TAD borders. Knockdown of SDC-2, the hermaphrodite specific DCC subunit required for condensin DC recruitment to the X or deletion of the *rex* sequences, eliminated the TAD borders that overlap with the *rex* sites [43, 44]. A catalytically inactive DPY-21, histone

H4K20me2 demethylase that interacts with condensin DC also weakened TAD borders [45], supporting the idea that condensin DC regulates the 3D organization of the X chromosomes in *C. elegans*.

Here we addressed the mechanism by which *rex* sites and condensin DC form TADs. We found that inserting three *rex* sites on chromosome II forms a loop anchored TAD-like domain. Condensin DC spreads bidirectionally from the ectopically inserted *rex*es over long distance. Supporting the idea that condensin DC recruitment is critical for insulation of DNA contacts by a *rex* site, spreading of condensin DC to the autosomal region of the X;V fusion chromosome increased 3D contacts, but failed to form TADs. A majority of the *rex* sites, including all that act as TAD borders, contain a 12-bp DNA sequence motif present in multiple copies. Insertion of a motif containing strong *rex* in two opposing orientations lead to formation of loop-anchored TADs with similar looping contacts, suggesting that motif orientation is not important for the function of the *rex* sites. To understand how condensin DC translocates along the chromosome, we targeted a dCas9-Suntag complex to a region of the X containing repeat DNA. Condensin DC accumulated at the block, supporting the loop extrusion hypothesis. In summary, our results support a model whereby loop-anchored TADs on the X are formed by condensin DC mediating 3D DNA contacts through loop extrusion and strong *rex* sites promoting and insulating these contacts through recruitment and bidirectional spreading of condensin DC molecules.

Materials & Methods

All sequencing data are available at Gene Expression Omnibus under GSE168803.

Strains

Unless otherwise noted, strains were grown on NGM media under standard worm culturing conditions. N2 wild type, one rex insertion ERC06 (knuSi254[SNP400bprex-1, unc-119(+)] II; unc-119(ed3) III), two rex insertion ERC62 (ersIs26[X:11093923-11094322[rex-8], II: 8449965); knuSi254[SNP400bprex-1, unc-119(+)] II; unc-119(ed3) III), 3 rex insertion ERC63 (ersIs27[X:11093923-11094322[rex-8], II:8371600, II:8449968); knuSi254[SNP400bprex-1, unc-119(+)] II; unc-119(ed3) III), and 8 rex insertion ERC08 (knuIs6[pSE-02(400bprex-1SNP), unc-119(+))] I; unc-119(ed3) III) strains were previously described [35]. Upstream oriented rex-8 insertion strain is ERC69 (ersIs33[X:11093924-11094281[rex-8], X:14373128]), downstream oriented insertion ERC80 (ersIs52[X:11094281-11093924[rex-8reverse], X:14373128]). X-V fusion YTP47 (XR-VR) and condensin DC spreading was described in [39]. Primer sequences used in the generation of the CRISPR strains are included in Supplemental File 1.

Constructs and transgenes

dCas9-Suntag targeting strain containing the sgRNA is JZ2005 with the genotype pySi27[Pfib-1:NLS::scFv::sfGFP::NLS::tbb-2 3'UTR /unc-119(+)] I; pySi26[Pfib-1::NLS::dCas9::24xGCN4::NLS::tbb-2 3'UTR /unc-119(+)] II; unc-119(ed3)/+ III; pyIs1002(pU6::sgRNA- X227/Punc-122::mCherry), and without the sgRNA is JZ1973

(pySi[Pfib-1:NLS:scFv:sfGFP/unc-119(+)] I; pySi[Pfib-1:NLS:dCas9:24xGCN4/unc-119(+)] II; unc-119(ed3) III).

pNLZ10 (Pfib-1::NLS::dCas9::24xGCN4::NLS::tbb-2 3'UTR) construct contains pCFJ150 vector backbone (Addgene plasmid # 19329). *SV40* NLS::dCas9::*egl-13* NLS:: tbb-2 3'UTR was derived from pJW1231 (Phsp-16.48::NLS::dCas9::EGFP::NLS::tbb-2 3'UTR) (a generous gift from Dr. Jordan D Ward), which was made by introducing D10A and H840A mutations into pMB66 (Phsp-16.48:NLS:Cas9:EGFP:NLS:tbb-2 3'UTR)[46]. To produce catalytically dead Cas9 (dCas9) and then subcloned into pCFJ150 vector. NLS: nuclear localization signal. A codon-optimized 6.25 copies of GCN4 fragment [47] was synthesized by IDT, and another 3 multiple GCN4 fragments containing artificial introns were made by PCR amplification to generate 24 copies of GCN4.

pNLZ11 (Pfib-1::NLS::scFv::sfGFP::NLS::tbb-2 3'UTR) construct has the pCFJ210 vector backbone (Addgene plasmid # 19329). A codon-optimized scFv::sfGFP fragment [47] was ordered from IDT. *fib-1* promoter was PCR amplified from worm genomic DNA. *tbb-2* 3'UTR was amplified from pJW1231 (Phsp-16.48::NLS::dCas9::EGFP::NLS::tbb-2 3'UTR). *SV40* and *egl-13* NLS sequences were added with PCR primers used for amplifying assembly fragments.

pBHC1131 (PU6::sgRNA-X227) construct (a generous gift from Baohui Chen) was derived from pDD162 (Addgene plasmid #47549) [48] and targets an X chromosome repetitive region with guide RNA sequence 5'-GGCGCCCATTTAAGGGTA-3'. The sgRNA construct was modified with optimized sgRNA scaffold (F+E) which can improve the CRISPR imaging efficiency in human cells [49].

Pfib-1::NLS::dCas9::24xGCN4::NLS::tbb-2 3'UTR and Pfib-1::NLS::scFv::sfGFP::NLS::tbb-2 3'UTR were single-copy inserted into worm genome by MosSCI using direct injection protocol [50]. PU6::sgRNA-X227 was injected at 200 ng/uL concentration with P*unc-122*::mCherry as the co-injection marker to get a transgenic extrachromosomal array line, which was subsequently integrated into worm genome by TMP-UV method.

ChIP-seq and mRNA-seq

ChIP-seq and mRNA-seq experiments were performed as previously described [35]. Antibody information and new and published data sets used are given in Supplemental File1. ChIP-chip data from Ercan et al 2009 was processed by centering average background enrichment to 0, normalizing to unity and multiplying by a constant to increase y-axis values. We aligned 50-75bp single-end ChIP-seq reads to *C. elegans* genome version WS220 using bowtie2 2.3.2 with default parameters [51]. Bam files were then sorted and indexed using samtools version 2.1.1 [52]. ChIP enrichment was normalized by dividing to input using DeepTools bamCompare using the following parameters: CPM, bin-size of 10bp, ignore duplicates, extend reads to 200bp, exclude chrM and remove blacklisted regions [53]. For analyzing ChIP-seq data across the X chromosomal repeat block, --very sensitive option was used in bowtie2 and --minMappingQuality was removed for bamCompare. MACS2 version 2.1.1 was used for fragment size prediction and for peak calling. For single replicate peak calling a minimum false discovery rate of .05 was used and

for merged replicates a minimum false discovery rate of .01 was used. Bedtools intersect was used to determine overlapping peaks between replicates and only those present in the majority of the replicates were chosen as final peaks.

Hi-C

Worms were grown on standard NGM plates and gravid adults were bleached to obtain embryos, which were crosslinked with 2% formaldehyde and stored at -80C . Frozen embryos were then resuspended in and crosslinked with 2% formaldehyde in M9 for another 30 mins. The embryos were spun down at 6000g for 30 sec and washed once with 100mM Tris Cl pH 7.5 and twice with M9. The embryo pellet was resuspended in 1 ml embryo buffer (110 mM NaCl, 40 mM KCl, 2 mM CaCl2, 2 mM MgCl2, 25 mM HEPES-KOH pH 7.5) containing 1 unit chitinase (Sigma), digested approximately 15 minutes, blastomeres were washed with embryo buffer twice by spinning at 1000g 5 min. The pellet was resuspended in Nuclei Buffer A (15 mM Tris–HCl pH 7.5, 2 mM MgCl2,0.34 M Sucrose,0.15 mM Spermine, 0.5 mM Spermidine, 1 mM DTT,0.5 mM PMSF (1X Calbiochem Protease Inhibitor cocktail I), 0.25% NP-40, 0.1% Triton X-100), centrifuged at 1000g for 5 minutes at 4C then resuspended in 1.5 mL Nuclei Buffer A. The embryos were then dounced 10X with a loose pestle and 10X with a tight pestle. The nuclei were separated from the cellular debris through spinning down the dounced material at 200G, then collecting the supernatant containing the nuclei into a separate tube. The pellet was resuspended in 1.5mL and the douncing process was repeated four times. Each individual supernatant containing nuclei was checked for quality by DAPI staining and those without debris were pooled and spun down at 1000G for 10 mins at 4C. Approximately 20 ul nuclei pellet were used to proceed to Arima Hi-C per the manufacturer's instructions. Library preparation was performed using the KAPA Hyper Prep Kit using the protocol provided by Arima. Paired-end Illumina sequencing was performed with Nextseq or Novaseq.

Paired end Illumina sequence reads were mapped using default parameters of the juicer pipeline (version=1.5.7) as described in [54]. For insertions and fusion strains, the reference genome was modified to match the genetic changes. For downstream analysis, inter_30.hic outputs from juicer pipeline were converted to h5 file to be used in HiCExplorer (version=3.5.1) [55, 56]. Matrices of replicates were combined using hicSumMatrices. Each replicate or each summed matrix were normalized to match the depth of the smallest matrix in comparison using hicNormalize with the option --smallest. The replicate and summed matrices were ICE normalized using hicCorrectMatrix with the following parameters: --correction_method ICE, -t 1.7 5, --skipDiagonal, --chromosomes I II III IV V X or I II III IV XV for X-V fusion.

The insulation scores were computed using the 10kb-binned normalized matrix function hicFindTADs with the following parameters: --correctForMultipleTesting fdr, --minDepth 80000, --maxDepth 200000, --step 40000. For 2kb-binned normalized matrix, the following parameters were used: --correctForMultipleTesting fdr, --minDepth 16000, --maxDepth 40000, --step 8000. Output score.bedgraph was compared between experimental conditions. The bedgraph file was converted to bigwig using BedgraphToBigwig utility provided from UCSC website [57].

In silico 4C plots were generated using the chicViewpoint function of hicexplorer with the following parameters: --averageContactBin 3 --range 20000000 20000000. The plotted values indicate relative contact scores out of 1000. The background model for chicViewpoint was generated using the summed wildtype matrix using the chicViewpointBackgroundModel function.

Results

Condensin DC spreads bidirectionally from ectopically inserted rex sequences on autosomes

In previous work, we showed that insertion of a single *rex* to autosomes fails to recruit condensin DC, but insertion of additional *rex*es at a distance of ~30-50kb increases condensin DC binding as measured by ChIP-qPCR [35]. Others have shown that insertion of 3 *rex* sites 1.4Mb apart over a 2.8Mb region onto autosomes failed to establish a TAD border [44]. We reasoned that failure to do so might have been the failure of these sites to cooperate over Mb distances to recruit enough condensin DC. Thus, we revisited the question of if *rex* sites can form TAD borders and sought to test if and how *rex* insertions that are capable of recruiting condensin DC as measured by qChIP are able to create condensin DC bound TADs.

We analyzed condensin DC binding by performing DPY-27 ChIP-seq in two strains [35]. The first strain was generated by serial insertion of one *rex-1* (intermediate strength rex) and two *rex-8* (strong *rex*) on chromosome II by MosSci and CRISPR, respectively. The three *rex* sites exist within a ~80Kb stretch of DNA. The sequential insertion of *rex* sites generated intermediate strains containing one or two *rex* sites, allowing us to observe the cooperative condensin DC recruitment to the same genomic region. The second strain was generated via integration of an extrachromosomal array of a plasmid containing *rex-1* in eight copies on chromosome I.

First, we analyzed how condensin DC spread from the inserted *rex* elements on chr II and chr I (Figure 1A). Upon single *rex-1* insertion on chromosome II, the ChIP-seq profile did not differ much from no insertion. Upon insertion of the second *rex* approximately 30Kb downstream of the first, condensin DC binding increased surrounding the insertions. The strain harboring three *rex* sites supported higher condensin DC binding, with peaks enriched at promoters, similar to that of the X chromosome (Figure 1A, bottom panel). DPY-27 ChIP-seq enrichment was elevated ~200kb surrounding the insertions while peaks unique to the three-*rex* strain extended to ~1 Mb region around the ~80kb insertion site, indicating that condensin DC is capable of spreading bidirectionally over long distances from the inserted *rex* sites.

The spreading from the 8-*rex* insertion on chromosome I was also similar (Figure 1B). In both cases, the level of binding around the ectopic *rex* insertions was less than on the X (Supplemental Figure 1A) suggesting that presence of multiple *rex* sites confers robust condensin DC binding on the X (Figure 1C). In summary, analysis of condensin DC binding

upon ectopic *rex* insertion indicates that spreading of condensin DC from the *rex* sites is bidirectional.

Condensin DC binding effects on domain-level gene repression

Robust recruitment of condensin DC on the X chromosomes results in chromosome-wide repression of transcription by a factor of ~2 [32-34]. Supporting the idea that condensin DC binding represses transcription, on X-A fusion chromosomes, condensin DC spreading into the autosome leads to gene repression in a manner proportional to condensin DC binding [41]. We performed mRNA-seq in the *rex* insertion strains and observed that genes were not consistently and individually repressed based on local DCC binding (Figure 2D). However, when expression changes are analyzed at the domain level within 200 or 500 kb bins, repression was more apparent.

In the 3-*rex* strain, gene expression within the bin containing the *rex* insertions showed a downward trend but this was not statistically significant (Supplemental Figure 1B). In the 8-*rex* strain, the 500 kb bin containing the *rex* insertions was significantly repressed relative to the rest of chromosome I (Supplemental Figure 1B). It is notable that qChIP analysis had shown higher recruitment by the 8-*rex* compared to the 3-*rex* insertion [35]. Lastly, chromosome-wide expression showed a downward trend for the chromosome harboring the *rex* insertion, but the effect sizes were small (Figure 1E). Overall, expression analyses support the idea that condensin DC creates repressive domains whose effect size is proportional to the level of condensin DC binding at these domains.

Ectopic rex insertions on chromosome II form a loop-anchored TAD

To test if *rex* sites that recruit condensin DC can form TAD borders on autosomes, we performed Hi-C analysis in the 3-*rex* strain, where the two inserted rexes are *rex-8*, which acts as a TAD border on the X [44]. We found that the two distal *rex-8* insertions spaced approximately 80Kb apart had an increase in interaction frequency suggesting that these two sites are forming a loop where previously there was no interaction in this region of chromosome II in wildtype animals (Figure 2A). The interaction between the weaker *rex-1* and the strong *rex-8* sites is harder to assess by Hi-C since this site is close to each *rex-8* (Figure 2B). To further analyze *rex-1* interactions, we used *in silico* 4C with each inserted *rex* as a bait. We found that relative to the wild type, all 3 *rex* insertion sites interacted with each other (Figure 2C). Additionally, there was a reduction in insulation score at the insertion sites, indicating increased insulation of 3D contacts across the ectopic *rex*es. These results are consistent with the hypothesis that TAD insulation activity of *rex* sites requires condensin DC recruitment, and that *rex* sites that recruit condensin are sufficient to form loop-anchored TADs on autosomes.

Inserting rex-8 in two different orientations leads to similar 3D looping interactions with the surrounding rex sites

The fact that strong *rex* sequences containing the 12-bp DNA motif form TAD boundaries lead us to test if they act analogously to CTCF sites in mammals. CTCF motif orientation is important for TAD border establishment [58-60]. To address if *rex* sites are analogous to CTCF binding sites, we generated two strains in which a single copy of *rex-8* was inserted on the X chromosome at the same location in two directions (Figure 3A). *Rex-8* was shown

to be sufficient for TAD establishment on the X [43, 44] and contains four motifs within a 200 bp sequence all in the same orientation. Condensin DC binding patterns across the X were similar between the two insertion strains (Figure 3B) and DPY-27 ChIP-seq enrichment indicated that the two insertions recruited similar levels of condensin DC relative to the other *rex*es (Figure 3C).

We performed Hi-C and compared the resulting matrices between wildtype and both insertion strains. In both orientations, the inserted *rex-8* sequence was able to establish a novel TAD border and loop with the neighboring *rex*es (Figure 3A), thus motif orientation does not control specificity of *rex* interactions. Insulation scores across the insertion site were consistently lower in the replicates of data from both insertion strains (Supplemental Figure 3), thus the inserted *rex-8* similarly regulates 3D DNA contacts regardless of its orientation. These results indicate that strong *rex* sites act as insulators regardless of motif orientation.

TAD formation requires condensin DC recruitment by the rex sequences

Next, we asked if condensin DC binding or *rex* sequences are responsible for the establishment of TADs on the X. To address this question, we performed Hi-C in a strain containing X;V fusion chromosomes, where condensin DC spreads ~3 Mb into V but no new recruitment sites are generated [39]. 3D DNA contacts were increased across the fusion site, which is expected for the chromatin polymer (Figure 4A). Consistent with the idea that condensin DC binding increases long-range 3D contacts, the autosomal spreading region showed an increase in DNA contacts measured by Hi-C (Figure 4B). There were no new dips in the insulation score along the region of spreading (Figure 4A). These results suggest that condensin DC binding increases chromatin contacts, but recruitment by *rex* sequences are needed for insulation to create TAD borders.

Off note, the replicates of Hi-C in the X;V strain were performed using different crosslinking conditions. In Figure 4, the experiment was performed using live-crosslinked embryos stored frozen, followed by a second crosslink before carrying out Hi-C. In supplemental Figure 4, the experiment was performed using single live crosslinking. The background interactions in the Hi-C are lower when double cross linking is used (Supplemental File 1). Nevertheless, the main results from the replicates concurred. There were no new TAD borders while 3D contacts at the autosomal region increased in the X;V fusion (Supplemental Figure 4). Thus, condensin DC binding increases 3D contacts, but in the absence of recruitment by a *rex* site, no new loop-anchored TADs are created.

Condensin DC accumulates at a dCas9 generated block on the X chromosome

While it is clear that condensin DC spreads linearly along the chromosome [39], it is not clear if the molecular mechanism by which condensin DC spreads is through loop extrusion. To address this question, we wondered if a large block on the chromatin fiber possibly extruding from the diameter of ~40 nM of condensin ring could prevent condensin DC translocation along chromatin. The rationale was based on *in vitro* work showing that linear translocation of cohesin can be blocked using a dCas9-mediated protein obstacle [61].

To address if linear spreading of condensin DC can be blocked, we utilized a dCas9 based system in which dCas9-Sun tag and binding proteins are expressed in presence of an sgRNA targeting a repetitive region of the X chromosome (Figure 5A). The relative size of each individual protein complex (dCas9-Suntag + Pfib-1:NLS:scFv-GFP) is approximately 1400kDa and is predicted to be larger than the ~20nm blocks used for *in vitro* experiments [61]. In addition to the size of the block being large enough to block spreading, we utilized a repetitive region as the target so that multiple blocking complexes could be recruited to a relatively small genomic locus. We confirmed that dCas9 was targeted to the repeat region in the presence of the sgRNA using ChIP-seq (Figure 5B). Strikingly, dCas9 targeting this region increased condensin DC binding, supporting the idea that the large dCas9-Suntag complex acts as a block to condensin DC translocation along DNA (Figure 5B).

To evaluate if 3D genome organization was affected by the block, we performed Hi-C and saw that the genome architecture was largely unaltered (Figure 5B). DPY-27 and GFP ChIP-seq profiles are plotted under the Hi-C to indicate the site of the dCas9-Suntag-scFv-GFP block. There was a slight increase in Hi-C insulation at the block site, but the repeat region already has some insulation activity in the wild type. It is possible that blocking condensin DC is not sufficient for insulation and *rex* sequences are required. Nevertheless, our results support the idea that a physical protein block of sufficient size is capable of affecting condensin DC's linear translocation, thus providing *in vivo* evidence for loop extrusion hypothesis for a metazoan condensin.

Discussion

The current model of condensin DC binding to the X chromosomes involves a two-step mechanism of recruitment and spreading [31]. X-specific recruitment is accomplished by ~64 *rex* sites, the majority of which include multiple copies of a 12-bp sequence motif, required for their function [35-38]. It is not clear what protein binds directly to these motifs, but other DCC subunits, including SDC-1, SDC-2 and DPY-30 are required condensin DC recruitment to the X chromosome [31, 62]. Work in other condensins and bacterial SMC complexes points to a similar mechanism in regard to DNA binding: recruitment or the initial nucleation through interactions with proteins bound at specific sites followed by linear spreading along DNA [63-65]. Here, X-specificity of condensin DC binding and ability to engineer recruitment elements in the genome allowed us to address how a metazoan condensin's recruitment and spreading regulates 3D organization of chromosomes.

How does the recruitment sites establish condensin DC binding domains?

On the X chromosome, deletion of a single *rex* site reduced condensin DC binding over ~1 Mb domain by about ~20-40%, suggesting that multiple recruitment sites contribute condensin DC across long distances to establish robust condensin DC binding across the X chromosome [35]. In agreement with this conclusion, we found that insertion of *rex* elements on autosomes create large domains of condensin DC binding (Figure 1). The fact that binding surrounds the *rex* insertions indicates that condensin DC can spread from the recruitment elements in either direction and over distances exceeding hundreds of kilobases. Since insertion of one or two *rex* sites did not noticeably increase condensin DC binding, establishing a condensin DC binding domain does not linearly correlate with the

number of *rex* sites, but requires passing a threshold due to cooperative nature of the recruitment and/or spreading.

What is the molecular mechanism of condensin DC spreading from the rex sites?
Our results support the loop extrusion hypothesis, where a dCas9-Suntag-scFv-GFP complex blocked the translocation of condensin DC along DNA (Figure 5). Processivity of the complex could determine the rate of reduction in binding away from the *rex* sites, as seen in the ectopic insertion experiments here and in X:A fusion chromosomes [39, 41]. In X;A fusion chromosomes, condensin DC spreads over 1-3 Mb distances covering hundreds of active genes and the ~1Mb ribosomal DNA repeats on chr X;I [39]. Thus, the process of loop extrusion should at some rate overcome large blocks. This is supported by the observation that cohesin complexes were capable of traversing a strong block albeit at a lower frequency [66]. One possibility is that condensin DC loop extrusion is a combination of continuous and discontinuous movement along the chromosome.

Bidirectional spreading from the recruitment sites using a loop extrusion mechanism may be a conserved feature of condensin activity, as *in silico* modeling found bidirectionality as an important feature to support proper mitotic chromosome compaction [67] and *in vitro* analysis showed bidirectional movement of mammalian condensins [18, 20]. In *B. subtilis*, the SMC complex is loaded by ParB to ParS sites and spreads to the arms of the bacterial chromosome in a bidirectional manner, juxtaposing the two arms together [68, 69]. A closer look at the *rex* sites in the Hi-C data does not reveal a similar "hairpin" structure (Figure 2,3). Instead, it is possible that condensin DC can enter and start moving in either direction from the *rex* sites. The lack of strong stripes from the *rex* sites suggests that there is high heterogeneity of DNA loops formed after movement from the *rex* sites in embryos.

How do rex sites create loop-anchored TADs?
Previous work showed that a subset of strong *rex* sites creates loop-anchored TADs [43, 44]. Here, we showed that condensin DC binding in itself does not create TAD borders but requires *rex* sites (Figure 4). How do strong *rex* sites create TAD borders? A single *rex* insertion on an autosome, which is expected to not recruit enough condensin DC, is incapable of forming a TAD border [44]. While three *rex* insertions on chromosome II recruited condensin DC and showed insulation activity (Figure 2). We previously noted that strong *rex* sites reduce condensin DC spreading [35]. Thus, we propose that the *rex* sites' insulation activity is based on the condensin DC molecules inability to pass over others being loaded and moving out from the *rex* sites. Such a clash between condensins have been suggested for the *B. subtilis* SMC complex, and may be a conserved feature of condensins [70, 71].

Alternatively, presence of large protein complexes at the *rex* sites may slow down or reduce the passage of condensin DC. Inducible loading of the bacterial SMCs followed by ChIP-seq and Hi-C analysis measured the speed of complex movement on DNA in the order of hundreds to a kilobase per second [68, 72], which is in a similar range as *in vitro* speed of loop extrusion by eukaryotic condensins [18-20, 73]. Notably, bacterial SMC complex speed *in vivo* reduces through a head on conflict with transcription [68, 72, 74]. Condensin DC accumulation at promoters suggest that similar factors may be in play in *C. elegans* [36, 41].

In a third possibility, specific proteins bound at the *rex* sites may physically interact to block condensin DC [75-80]. In *Caenorhabditis*, a CTCF ortholog is not present [81], however, SDC-2 transcription factor and two zinc finger containing proteins, SDC-3 and SDC-1, and DPY-30 a subunit of the COMPASS complex are required for the recruitment of condensin DC to the X [31]. CTCF binding in a convergent orientation regulates its protein interaction domains that prevent cohesin translocation [79, 82-85]. Since 12-bp motif orientation does not influence the specificity of the inserted *rex* sites making loops with surrounding *rex* sites (Figure 3), it is possible that the responsible protein(s) act as non-CTCF insulators like Zelda or share similar insulating properties and may facilitate TAD establishment such as YY1, which do not require a specific motif orientation [86-89].

How do rex sites that are more than Mb distance away form loops?

It is possible that condensin DC loop extrusion from one *rex* to the other form a loop or that other proteins mediate the long-range interactions between *rex*es. The catalytic mutation in the H4K20me2 demethylase DPY-21, which is part of the DCC reduces looping between *rex* sites [45]. Thus, a combination of both models is possible, where initial proximity of the *rex*es created by condensin DC loop extrusion could be reinforced by condensin DC molecules that can hold the two *rex* sites, similar to how yeast condensin mediates interaction between tRNA genes on different chromosomes [90].

It is not clear if there is a function for looping between *rex* sites. Deletion of eight strong *rex* sites eliminated the specific loops on the X, yet did not affect dosage compensation [44]. However, it remains unknown if looping provides some robustness to the system by putting *rex* sites together in close proximity to increase local concentration of the complex, which may be more important during the establishment of dosage compensation in early embryogenesis or its maintenance as chromatin features are challenged upon stress or during aging.

C. elegans dosage compensation system co-opting a condensin complex required the evolution of X-specific condensin recruitment sites, opening a window into how eukaryotic condensins enter and move along chromosomes *in vivo*. Here our work supports a model in which condensin DC is loaded at and spreads bidirectionally from the *rex* sites translocating along chromatin over hundreds of kilobase distances (Figure 6). Insulator proteins that bind to the strong *rex* sites or clash of incoming condensin DC molecules with those coming off the *rex* sites, create loop-anchored TAD borders. It is not clear if and how condensin-DC mediated 3D structure of the chromosome contributes to transcription repression. Future work addressing this question will reveal more insights into the function of condensin-mediated genome organization.

Figure Legends

Figure 1 *Condensin DC spreads over hundreds of kb distance bidirectionally from ectopically inserted rex sequences* A) DPY-27 ChIP-seq/input ratio data comparing wild-type average with a single intermediate *rex-1* insertion (grey) on chromosome II, a subsequent strong *rex-8* insertion (pink) 30 Kb downstream from *rex-1* and a second copy of *rex-8* inserted 50 Kb upstream from *rex-1*. Schematic depicting the *rex* site insertions on chromosome II are shown next to each respective strain's ChIP-seq/input data track. In the bottom panel, a 100 Kb window centered around the insertion site for chromosome II is shown. Gene tracks are displayed below. B) Schematic depicting the inserted array containing 8 copies of *rex-1* on chromosome I. DPY-27 ChIP-seq/input ratio data comparing wild-type and insertion strain is shown within a 2 Mb window centered around the estimated insertion region. C) Violin plots showing condensin DC binding measured by DPY-27 ChIP-seq/input for the 3 *rex* insertion strain and the 8 *rex* insertion strain. ChIP-seq/input scores at peaks within a 200 Kb window surrounding the insertion sites were plotted and compared to condensin DC binding at peaks on the X chromosome for both strains. D) mRNA-seq data comparing the 3-*rex* insertion strains to wildtype is shown. The points indicate log2 fold change between the insertion and wildtype for each gene. Grey shading underneath the points indicate gene bodies and the *rex* insertions are annotated. The displayed window is a 100Kb region centered around the central insertion for the 3 *rex* insertion strain and a 50Kb region centered around the insertion for the 8 *rex* insertion strain. E) Boxplots of the log2 fold change in the 3-*rex* (left panel) and 8-*rex* strains(right panel). Autosomes III, IV & V are binned together, chromosomes I & X are shown as controls. Two-tailed student's t-test p-values are given.

Supplemental Figure 1 *Condensin DC binding at the ectopic autosomal spreading regions are lower than that of the X and lead to a slight reduction in domain-wide gene expression* A) DPY-27 ChIP-seq/input ratio data comparing wild-type average with a single intermediate *rex-1* insertion (grey) on chromosome II, a subsequent strong *rex-8* insertion (pink) 30 Kb downstream from *rex-1* and a second copy of *rex-8* inserted 50 Kb upstream from *rex-1*. Schematic depicting the *rex* site insertions on chromosome II are shown next to each respective strain's ChIP-seq/input data track. The 2 Mb window centered around the central insertion site and a similar region on the X chromosome are shown for comparison. DPY-27 binding peaks are shown below. B) log2 fold change ratios were averaged for genes within 200 Kb bins (top panels) and 500 Kb bins (bottom panels) tiled across chromosome II in the 3 rex and chromosome I in 8 rex insertion strains. Bins containing a significant level of repression are marked with asterisks (Fisher exact test p-value <.05 = *, p-value <.01 = **, p-value <.001 = ***) and red bins indicate bins that contain an inserted *rex* site.

Figure 2 *Inserted rex sites on chr II create loops and increase insulation of 3D DNA interactions* A) Heatmaps of Hi-C data binned at 2-kb resolution showing chromatin interaction frequencies for chromosome II in wildtype embryos (left panel) and in the 3-*rex* insertion strain (right panel). The red circle indicates a novel looping event. The arrows indicate increased insulation. B) The insulation scores for wild type and 3-*rex* harboring strain are shown in grey and red respectively. C) Hi-C data was used to generate *in silico* 4C-seq tracks for wildtype or 3-*rex* insertion strain embryos.

Figure 3 *Insertion of rex-8, which contains multiple 12-bp motifs in two opposite orientations form similar 3D DNA loops with surrounding rex sites* A) *Rex* sites and the orientation of the motifs surrounding the region in which *rex-8* is inserted in the 3' to 5' orientation or the 5' to 3' orientation. Dark arrows indicate high scoring 12-bp motifs [35](Albritton et al., 2017). Heatmaps of Hi-C data binned at 10-kb resolution showing chromatin interaction frequencies for chromosome X in wildtype embryos (left panel) 5' to 3' insertion harboring embryos (middle panel) and 3' to 5' insertion harboring embryos (right panel). DPY-27 ChIP-seq/input ratio and insulation scores are plotted for each strain. B) DPY-27 ChIP-seq/input ratio is shown for a comparable region on the X chromosome. C) Average DPY-27 ChIP-seq/input ratio was calculated for adjacent 150 bp windows around the 200 bp summit of each *rex* site. The level of DPY-27 binding at the ectopic *rex-8* (red) and other *rex*es are plotted against each other for comparing condensin DC recruitment in the two strains.

Supplemental Figure 3 *Insertion of rex-8, which contains multiple 12-bp motifs in two opposite orientations both show insulation effect at the insertion site but does not affect insulation elsewhere on the X.* Insulation scores of individual replicates are shown for the entire X chromosome in wild type and two *rex-8* insertion strains.

Figure 4 *Condensin DC binding increases 3D contacts but does not create new TADs in the absence of rex sites in autosomal spreading domain in the X;V fusion chromosomes* A) Heatmaps of Hi-C data binned at 50-kb resolution showing chromatin interaction frequencies for chromosome X and chromosome V. Wild type karyotype data is shown above the diagonal and fusion data is shown below the diagonal. Insulation scores are plotted below the heatmaps for wild type and X;V karyotypes in gray and green respectively. The *rex* sites are annotated and published DPY-27 ChIP-chip data are plotted. B)P(s,XV)/P(s,WT), fold change in Hi-C contact probability at various regions in the genome. While X;V-fusion did not form TADs, relative to the arms of other chromosomes, the fusion regions show increased interactions <300kb relative to interactions >300kb.

Supplemental Figure 4 *Hi-C data from single formaldehyde crosslink.* A) Heatmaps of Hi-C data binned at 50-kb resolution showing chromatin interaction frequencies for chromosome X and chromosome V. Wild type karyotype data is shown above the diagonal and fusion data is shown below the diagonal. Insulation scores are plotted below the heatmaps for wild type and X;V karyotypes in gray and green respectively. The *rex* sites are annotated and published DPY-27 ChIP-chip enrichment scores were normalized to unity and plotted. B)P(s,XV)/P(s,WT), fold change in Hi-C contact probability at various regions in the genome. While X;V-fusion did not form TADs, relative to the arms of other chromosomes, the fusion regions show increased interactions <300kb relative to interactions >300kb.

Figure 5 *Targeting dCas9 to a repeat region on the X chromosome leads to accumulation of condensin DC at the block site* A) Schematic depicting the multi-protein block and the

approximate size of the components utilized to prevent condensin from translocating linearly along chromatin. B) Zoomed in view of the 20kb region surrounding the target sites is shown. ChIP-seq of DPY-27 in the absence and presence of sgRNA targeting the repeat regions, and ChIP-seq of GFP targeting ScFv-dCas9 complex are shown. To visualize binding at the repetitive region, for this panel only, the reads were processed with less stringent parameters as detailed in methods. C) Heatmaps of Hi-C data binned at 50-kb resolution showing chromatin interaction frequencies for chromosome X in wildtype embryos (top heatmap) and in the block harboring strain (bottom heatmap). Insulation score and the nearby *rex*es are indicated. In the bottom panel, DPY-27 ChIP-seq/input ratios are plotted in a strain possessing the blocking components without an sgRNA (top track) and with the sgRNA (bottom track). The location of the block is annotated below the ChIP-seq data, and also marked by the GFP ChIP-seq against ScFv-dCas9 complex.

Figure 6 *A model for condensin DC recruitment, spreading and regulation of 3D organization of the chromosome* Our results support a model whereby *rex* sites serve as both condensin DC loading sites and as TAD borders. Loop extruding condensin DC molecules may clash with others that are loading and bidirectionally spreading from the *rex* sites. Orientation of the 12-bp motifs at the *rex* sites do not control the specificity of looping interactions and insulation activity. In summary, condensin DC mediated 3D DNA contacts combined with the insulation activity of the *rex* sites form the loop-anchored TADs on the X chromosomes.

Acknowledgements
SE and research in this manuscript was supported by the National Institute of General Medical Sciences of the National Institutes of Health under award numbers R01 GM107293 and R35 GM130311. DJ was supported in part by NIGMS Predoctoral Fellowship T32HD007520. We thank Dr. Noelle L'etoile, who generously supported Bo Zhang's postdoctoral work that included dCas9 targeting, with grants NIBIB R33 EB019784 and NIDCD R01 DC005991. We thank Jordan Ward and Baohui Chen for plasmids. We thank Gencore at the NYU Center for Genomics and Systems Biology. We also thank Shaun Mahony, Lila Rieber, Pedro Rocha, Ramya Raviram and Jane Skok who helped with experimental trials prior to adopting Hi-C, and Arima genomics for technical support.

Competing interests
None

References

1. Kumar, Y., D. Sengupta, and W. Bickmore, *Recent advances in the spatial organization of the mammalian genome.* J Biosci, 2020. **45**.
2. Rowley, M.J. and V.G. Corces, *Organizational principles of 3D genome architecture.* Nat Rev Genet, 2018. **19**(12): p. 789-800.
3. Stam, M., M. Tark-Dame, and P. Fransz, *3D genome organization: a role for phase separation and loop extrusion?* Curr Opin Plant Biol, 2019. **48**: p. 36-46.
4. Szalaj, P. and D. Plewczynski, *Three-dimensional organization and dynamics of the genome.* Cell Biol Toxicol, 2018. **34**(5): p. 381-404.
5. Gibcus, J.H., et al., *A pathway for mitotic chromosome formation.* Science, 2018. **359**(6376).
6. Naumova, N., et al., *Organization of the mitotic chromosome.* Science, 2013. **342**(6161): p. 948-53.
7. van Ruiten, M.S. and B.D. Rowland, *SMC Complexes: Universal DNA Looping Machines with Distinct Regulators.* Trends Genet, 2018. **34**(6): p. 477-487.
8. Wood, A.J., A.F. Severson, and B.J. Meyer, *Condensin and cohesin complexity: the expanding repertoire of functions.* Nat Rev Genet, 2010. **11**(6): p. 391-404.
9. Cuylen, S., J. Metz, and C.H. Haering, *Condensin structures chromosomal DNA through topological links.* Nat Struct Mol Biol, 2011. **18**(8): p. 894-901.
10. Minamino, M., et al., *Topological in vitro loading of the budding yeast cohesin ring onto DNA.* Life Sci Alliance, 2018. **1**(5).
11. Paul, M.R., A. Hochwagen, and S. Ercan, *Condensin action and compaction.* Curr Genet, 2019. **65**(2): p. 407-415.
12. Chang, L.H., S. Ghosh, and D. Noordermeer, *TADs and Their Borders: Free Movement or Building a Wall?* J Mol Biol, 2020. **432**(3): p. 643-652.
13. Dekker, J. and E. Heard, *Structural and functional diversity of Topologically Associating Domains.* FEBS Lett, 2015. **589**(20 Pt A): p. 2877-84.
14. Hansen, A.S., et al., *Recent evidence that TADs and chromatin loops are dynamic structures.* Nucleus, 2018. **9**(1): p. 20-32.
15. Kaiser, V.B. and C.A. Semple, *When TADs go bad: chromatin structure and nuclear organisation in human disease.* F1000Res, 2017. **6**.
16. Lupianez, D.G., M. Spielmann, and S. Mundlos, *Breaking TADs: How Alterations of Chromatin Domains Result in Disease.* Trends Genet, 2016. **32**(4): p. 225-237.
17. Camdere, G.O., K.K. Carlborg, and D. Koshland, *Intermediate step of cohesin's ATPase cycle allows cohesin to entrap DNA.* Proc Natl Acad Sci U S A, 2018. **115**(39): p. 9732-9737.
18. Kong, M., et al., *Human Condensin I and II Drive Extensive ATP-Dependent Compaction of Nucleosome-Bound DNA.* Mol Cell, 2020. **79**(1): p. 99-114 e9.
19. Ganji, M., et al., *Real-time imaging of DNA loop extrusion by condensin.* Science, 2018. **360**(6384): p. 102-105.
20. Terakawa, T., et al., *The condensin complex is a mechanochemical motor that translocates along DNA.* Science, 2017. **358**(6363): p. 672-676.
21. Nuebler, J., et al., *Chromatin organization by an interplay of loop extrusion and compartmental segregation.* Proc Natl Acad Sci U S A, 2018. **115**(29): p. E6697-E6706.

22. Gassler, J., et al., *A mechanism of cohesin-dependent loop extrusion organizes zygotic genome architecture.* EMBO J, 2017. **36**(24): p. 3600-3618.
23. Kim, Y., et al., *Human cohesin compacts DNA by loop extrusion.* Science, 2019. **366**(6471): p. 1345-1349.
24. Haarhuis, J.H.I., et al., *The Cohesin Release Factor WAPL Restricts Chromatin Loop Extension.* Cell, 2017. **169**(4): p. 693-707 e14.
25. Peters, J.M. and T. Nishiyama, *Sister chromatid cohesion.* Cold Spring Harb Perspect Biol, 2012. **4**(11).
26. Nora, E.P., et al., *Targeted Degradation of CTCF Decouples Local Insulation of Chromosome Domains from Genomic Compartmentalization.* Cell, 2017. **169**(5): p. 930-944 e22.
27. Rao, S.S., et al., *A 3D map of the human genome at kilobase resolution reveals principles of chromatin looping.* Cell, 2014. **159**(7): p. 1665-80.
28. D'Ambrosio, C., et al., *Identification of cis-acting sites for condensin loading onto budding yeast chromosomes.* Genes Dev, 2008. **22**(16): p. 2215-27.
29. Iwasaki, O., et al., *Interaction between TBP and Condensin Drives the Organization and Faithful Segregation of Mitotic Chromosomes.* Mol Cell, 2015. **59**(5): p. 755-67.
30. Csankovszki, G., et al., *Three distinct condensin complexes control C. elegans chromosome dynamics.* Curr Biol, 2009. **19**(1): p. 9-19.
31. Albritton, S.E. and S. Ercan, *Caenorhabditis elegans Dosage Compensation: Insights into Condensin-Mediated Gene Regulation.* Trends Genet, 2018. **34**(1): p. 41-53.
32. Kramer, M., P. Rao, and S. Ercan, *Untangling the Contributions of Sex-Specific Gene Regulation and X-Chromosome Dosage to Sex-Biased Gene Expression in Caenorhabditis elegans.* Genetics, 2016. **204**(1): p. 355-69.
33. Kramer, M., et al., *Developmental Dynamics of X-Chromosome Dosage Compensation by the DCC and H4K20me1 in C. elegans.* PLoS Genet, 2015. **11**(12): p. e1005698.
34. Kruesi, W.S., et al., *Condensin controls recruitment of RNA polymerase II to achieve nematode X-chromosome dosage compensation.* Elife, 2013. **2**: p. e00808.
35. Albritton, S.E., et al., *Cooperation between a hierarchical set of recruitment sites targets the X chromosome for dosage compensation.* Elife, 2017. **6**.
36. Ercan, S., et al., *X chromosome repression by localization of the C. elegans dosage compensation machinery to sites of transcription initiation.* Nat Genet, 2007. **39**(3): p. 403-8.
37. Jans, J., et al., *A condensin-like dosage compensation complex acts at a distance to control expression throughout the genome.* Genes Dev, 2009. **23**(5): p. 602-18.
38. McDonel, P., et al., *Clustered DNA motifs mark X chromosomes for repression by a dosage compensation complex.* Nature, 2006. **444**(7119): p. 614-8.
39. Ercan, S., L.L. Dick, and J.D. Lieb, *The C. elegans dosage compensation complex propagates dynamically and independently of X chromosome sequence.* Curr Biol, 2009. **19**(21): p. 1777-87.
40. Ercan, S. and J.D. Lieb, *C. elegans dosage compensation: a window into mechanisms of domain-scale gene regulation.* Chromosome Res, 2009. **17**(2): p. 215-27.
41. Street, L.A., et al., *Binding of an X-Specific Condensin Correlates with a Reduction in Active Histone Modifications at Gene Regulatory Elements.* Genetics, 2019. **212**(3): p. 729-742.

42. Vielle, A., et al., *H4K20me1 contributes to downregulation of X-linked genes for C. elegans dosage compensation.* PLoS Genet, 2012. **8**(9): p. e1002933.
43. Crane, E., et al., *Condensin-driven remodelling of X chromosome topology during dosage compensation.* Nature, 2015. **523**(7559): p. 240-4.
44. Anderson, E.C., et al., *X Chromosome Domain Architecture Regulates Caenorhabditis elegans Lifespan but Not Dosage Compensation.* Dev Cell, 2019. **51**(2): p. 192-207 e6.
45. Brejc, K., et al., *Dynamic Control of X Chromosome Conformation and Repression by a Histone H4K20 Demethylase.* Cell, 2017. **171**(1): p. 85-102 e23.
46. Waaijers, S., et al., *CRISPR/Cas9-targeted mutagenesis in Caenorhabditis elegans.* Genetics, 2013. **195**(3): p. 1187-91.
47. Tanenbaum, M.E., et al., *A protein-tagging system for signal amplification in gene expression and fluorescence imaging.* Cell, 2014. **159**(3): p. 635-46.
48. Dickinson, D.J., et al., *Engineering the Caenorhabditis elegans genome using Cas9-triggered homologous recombination.* Nat Methods, 2013. **10**(10): p. 1028-34.
49. Chen, B., et al., *Dynamic imaging of genomic loci in living human cells by an optimized CRISPR/Cas system.* Cell, 2013. **155**(7): p. 1479-91.
50. Frokjaer-Jensen, C., et al., *Single-copy insertion of transgenes in Caenorhabditis elegans.* Nat Genet, 2008. **40**(11): p. 1375-83.
51. Langmead, B. and S.L. Salzberg, *Fast gapped-read alignment with Bowtie 2.* Nat Methods, 2012. **9**(4): p. 357-9.
52. Ramirez-Gonzalez, R.H., et al., *Bio-samtools: Ruby bindings for SAMtools, a library for accessing BAM files containing high-throughput sequence alignments.* Source Code Biol Med, 2012. **7**(1): p. 6.
53. Ho, J.W., et al., *Comparative analysis of metazoan chromatin organization.* Nature, 2014. **512**(7515): p. 449-52.
54. Durand, N.C., et al., *Juicer Provides a One-Click System for Analyzing Loop-Resolution Hi-C Experiments.* Cell Syst, 2016. **3**(1): p. 95-8.
55. Wolff, J., et al., *Galaxy HiCExplorer: a web server for reproducible Hi-C data analysis, quality control and visualization.* Nucleic Acids Res, 2018. **46**(W1): p. W11-W16.
56. Ramirez, F., et al., *High-resolution TADs reveal DNA sequences underlying genome organization in flies.* Nat Commun, 2018. **9**(1): p. 189.
57. Kent, W.J., et al., *BigWig and BigBed: enabling browsing of large distributed datasets.* Bioinformatics, 2010. **26**(17): p. 2204-7.
58. Nanni, L., S. Ceri, and C. Logie, *Spatial patterns of CTCF sites define the anatomy of TADs and their boundaries.* Genome Biol, 2020. **21**(1): p. 197.
59. Nichols, M.H. and V.G. Corces, *A CTCF Code for 3D Genome Architecture.* Cell, 2015. **162**(4): p. 703-5.
60. Nishana, M., et al., *Defining the relative and combined contribution of CTCF and CTCFL to genomic regulation.* Genome Biol, 2020. **21**(1): p. 108.
61. Stigler, J., et al., *Single-Molecule Imaging Reveals a Collapsed Conformational State for DNA-Bound Cohesin.* Cell Rep, 2016. **15**(5): p. 988-998.
62. Meyer, B.J., *Sex and death: from cell fate specification to dynamic control of X-chromosome structure and gene expression.* Mol Biol Cell, 2018. **29**(22): p. 2616-2621.
63. Csankovszki, G., P. McDonel, and B.J. Meyer, *Recruitment and spreading of the C. elegans dosage compensation complex along X chromosomes.* Science, 2004. **303**(5661): p. 1182-5.

64. Li, Y., et al., *Structural basis for Scc3-dependent cohesin recruitment to chromatin.* Elife, 2018. **7**.
65. Wang, X., et al., *Bacillus subtilis SMC complexes juxtapose chromosome arms as they travel from origin to terminus.* Science, 2017. **355**(6324): p. 524-527.
66. Dequeker, B.J.H., et al., *MCM complexes are barriers that restrict cohesin-mediated loop extrusion.* bioRxiv, 2020: p. 2020.10.15.340356.
67. Banigan, E.J., et al., *Chromosome organization by one-sided and two-sided loop extrusion.* Elife, 2020. **9**.
68. Wang, X., et al., *In Vivo Evidence for ATPase-Dependent DNA Translocation by the Bacillus subtilis SMC Condensin Complex.* Mol Cell, 2018. **71**(5): p. 841-847 e5.
69. Wang, X., et al., *Condensin promotes the juxtaposition of DNA flanking its loading site in Bacillus subtilis.* Genes Dev, 2015. **29**(15): p. 1661-75.
70. Anchimiuk, A., et al., *Fine-tuning of the Smc flux facilitates chromosome organization in B. subtilis.* bioRxiv, 2020: p. 2020.12.04.411900.
71. Brandão, H.B., et al., *DNA-loop extruding SMC complexes can traverse one another in vivo.* bioRxiv, 2020: p. 2020.10.26.356329.
72. Tran, N.T., M.T. Laub, and T.B.K. Le, *SMC Progressively Aligns Chromosomal Arms in Caulobacter crescentus but Is Antagonized by Convergent Transcription.* Cell Rep, 2017. **20**(9): p. 2057-2071.
73. Strick, T.R., T. Kawaguchi, and T. Hirano, *Real-time detection of single-molecule DNA compaction by condensin I.* Curr Biol, 2004. **14**(10): p. 874-80.
74. Brandão, H.B., et al., *RNA polymerases as moving barriers to condensin loop extrusion.* Proceedings of the National Academy of Sciences, 2019. **116**(41): p. 20489-20499.
75. Hu, G., et al., *Systematic screening of CTCF binding partners identifies that BHLHE40 regulates CTCF genome-wide distribution and long-range chromatin interactions.* Nucleic Acids Res, 2020. **48**(17): p. 9606-9620.
76. Justice, M., et al., *A WIZ/Cohesin/CTCF Complex Anchors DNA Loops to Define Gene Expression and Cell Identity.* Cell Rep, 2020. **31**(2): p. 107503.
77. Lehman, B.J., et al., *Dynamic regulation of CTCF stability and sub-nuclear localization in response to stress.* PLoS Genet, 2021. **17**(1): p. e1009277.
78. Valletta, M., et al., *Exploring the Interaction between the SWI/SNF Chromatin Remodeling Complex and the Zinc Finger Factor CTCF.* Int J Mol Sci, 2020. **21**(23).
79. van Ruiten, M.S. and B.D. Rowland, *On the choreography of genome folding: A grand pas de deux of cohesin and CTCF.* Curr Opin Cell Biol, 2021. **70**: p. 84-90.
80. Xiao, T., X. Li, and G. Felsenfeld, *The Myc-associated zinc finger protein (MAZ) works together with CTCF to control cohesin positioning and genome organization.* Proc Natl Acad Sci U S A, 2021. **118**(7).
81. Heger, P., B. Marin, and E. Schierenberg, *Loss of the insulator protein CTCF during nematode evolution.* BMC Mol Biol, 2009. **10**: p. 84.
82. Debaugny, R.E. and J.A. Skok, *CTCF and CTCFL in cancer.* Curr Opin Genet Dev, 2020. **61**: p. 44-52.
83. Hansen, A.S., *CTCF as a boundary factor for cohesin-mediated loop extrusion: evidence for a multi-step mechanism.* Nucleus, 2020. **11**(1): p. 132-148.
84. Pugacheva, E.M., et al., *CTCF mediates chromatin looping via N-terminal domain-dependent cohesin retention.* Proc Natl Acad Sci U S A, 2020. **117**(4): p. 2020-2031.

85. Xiang, J.F. and V.G. Corces, *Regulation of 3D chromatin organization by CTCF.* Curr Opin Genet Dev, 2020. **67**: p. 33-40.
86. Hug, C.B., et al., *Chromatin Architecture Emerges during Zygotic Genome Activation Independent of Transcription.* Cell, 2017. **169**(2): p. 216-228 e19.
87. Li, M., et al., *Architectural proteins for the formation and maintenance of the 3D genome.* Sci China Life Sci, 2020. **63**(6): p. 795-810.
88. Lyu, X., M.J. Rowley, and V.G. Corces, *Architectural Proteins and Pluripotency Factors Cooperate to Orchestrate the Transcriptional Response of hESCs to Temperature Stress.* Mol Cell, 2018. **71**(6): p. 940-955 e7.
89. Weintraub, A.S., et al., *YY1 Is a Structural Regulator of Enhancer-Promoter Loops.* Cell, 2017. **171**(7): p. 1573-1588 e28.
90. Paul, M.R., et al., *Condensin Depletion Causes Genome Decompaction Without Altering the Level of Global Gene Expression in Saccharomyces cerevisiae.* Genetics, 2018. **210**(1): p. 331-344.

Figure 1

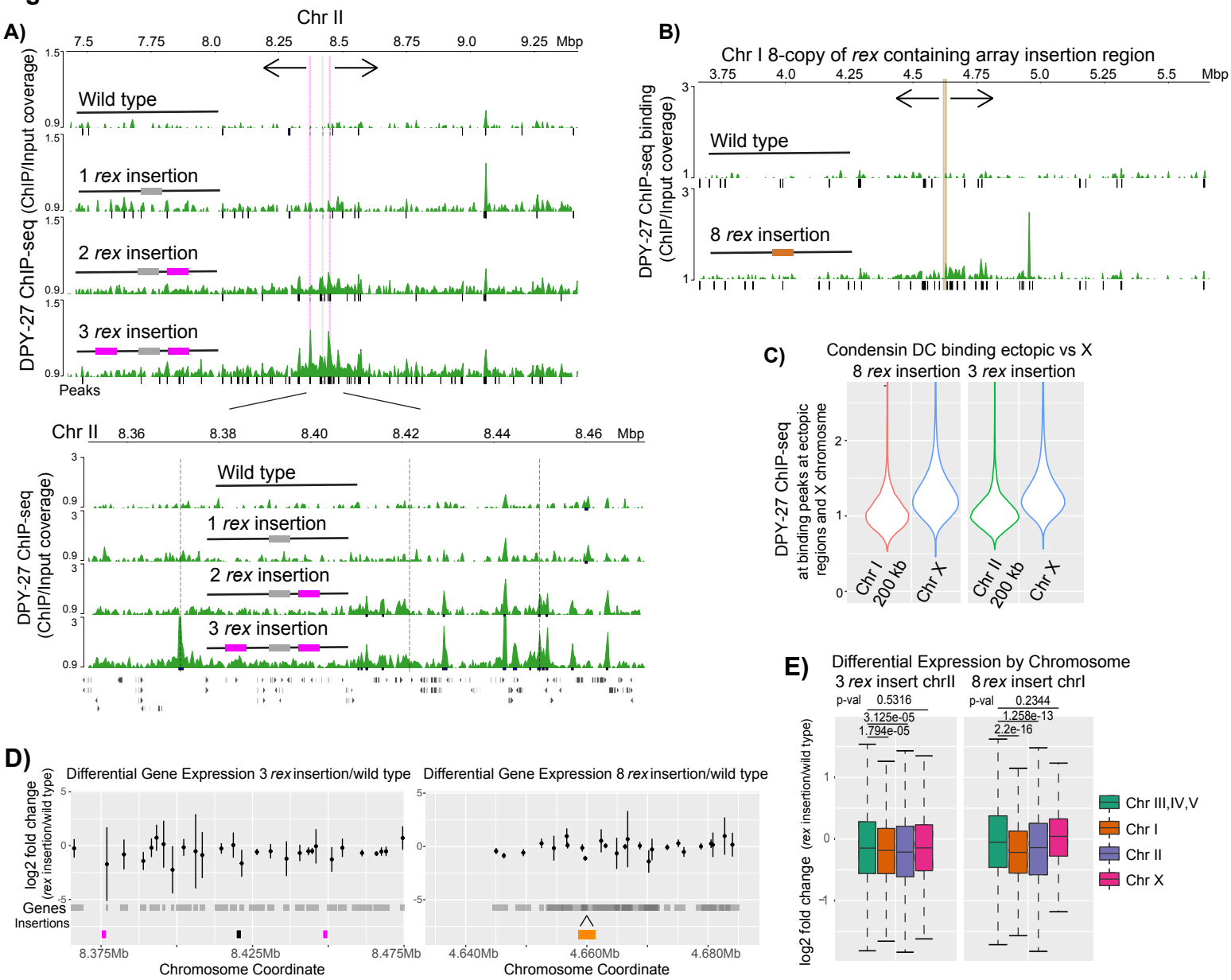
A)
Chr II
7.5 7.75 8.0 8.25 8.5 8.75 9.0 9.25 Mbp
DPY-27 ChIP-seq (ChIP/Input coverage)
Wild type
1 rex insertion
2 rex insertion
3 rex insertion
Peaks
Chr II 8.36 8.38 8.40 8.42 8.44 8.46 Mbp
DPY-27 ChIP-seq (ChIP/Input coverage)
B)
Chr I 8-copy of rex containing array insertion region
3.75 4.0 4.25 4.5 4.75 5.0 5.25 5.5 Mbp
DPY-27 ChIP-seq binding (ChIP/Input coverage)
Wild type
8 rex insertion
C)
Condensin DC binding ectopic vs X
8 rex insertion 3 rex insertion
DPY-27 ChIP-seq at binding peaks at ectopic regions and X chromosme
Chr I 200 kb
Chr X
Chr II 200 kb
Chr X
D)
Differential Gene Expression 3 rex insertion/wild type
Differential Gene Expression 8 rex insertion/wild type
log2 fold change (rex insertion/wild type)
Genes
Insertions
8.375Mb 8.425Mb 8.475Mb
4.640Mb 4.660Mb 4.680Mb
Chromosome Coordinate
E)
Differential Expression by Chromosome
3 rex insert chrII 8 rex insert chrI
p-val 0.5316
3.125e-05
1.794e-05
p-val 0.2344
1.258e-13
2.2e-16
log2 fold change (rex insertion/wild type)
Chr III,IV,V
Chr I
Chr II
Chr X

Figure 1 Supplement

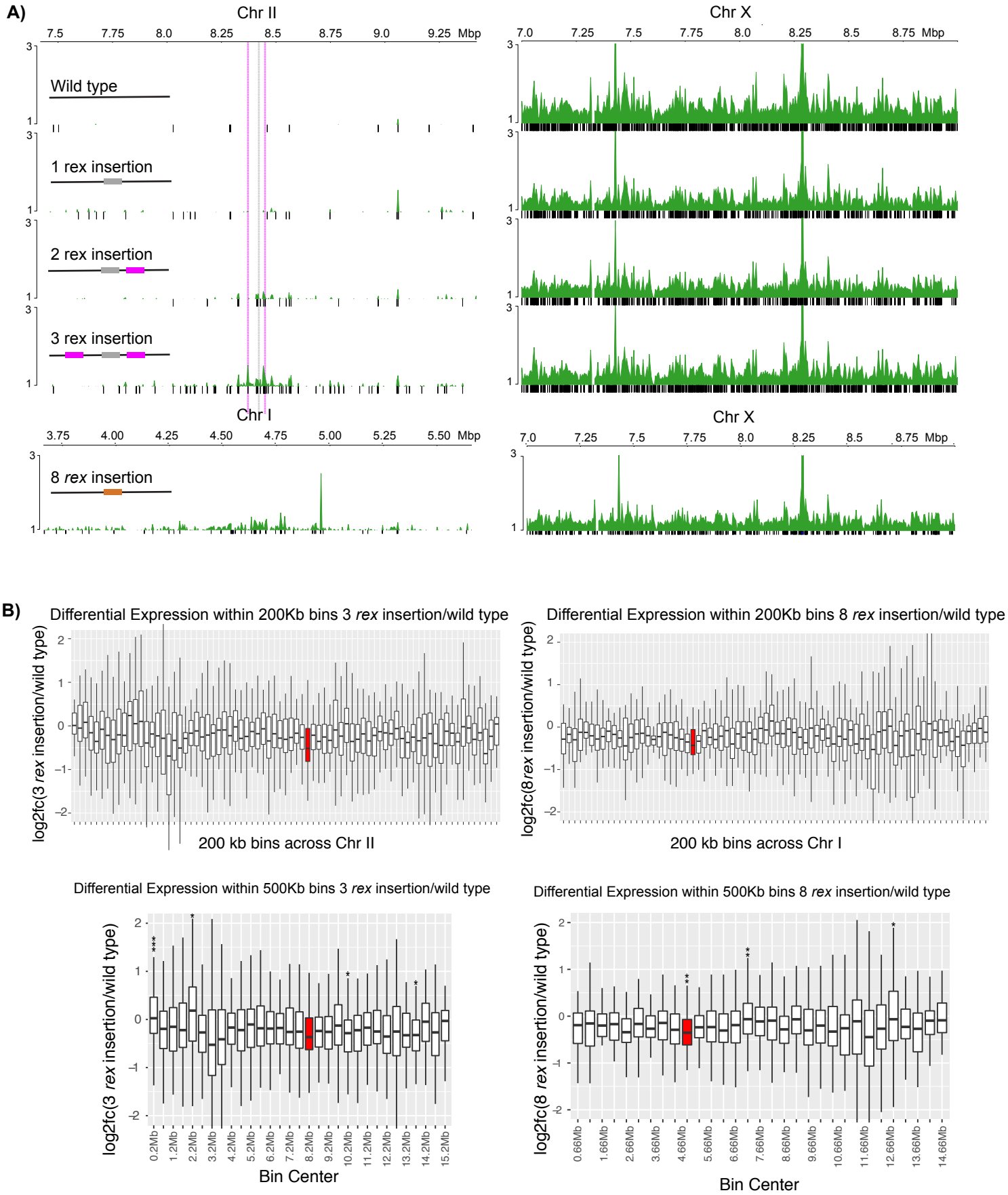

Figure 2

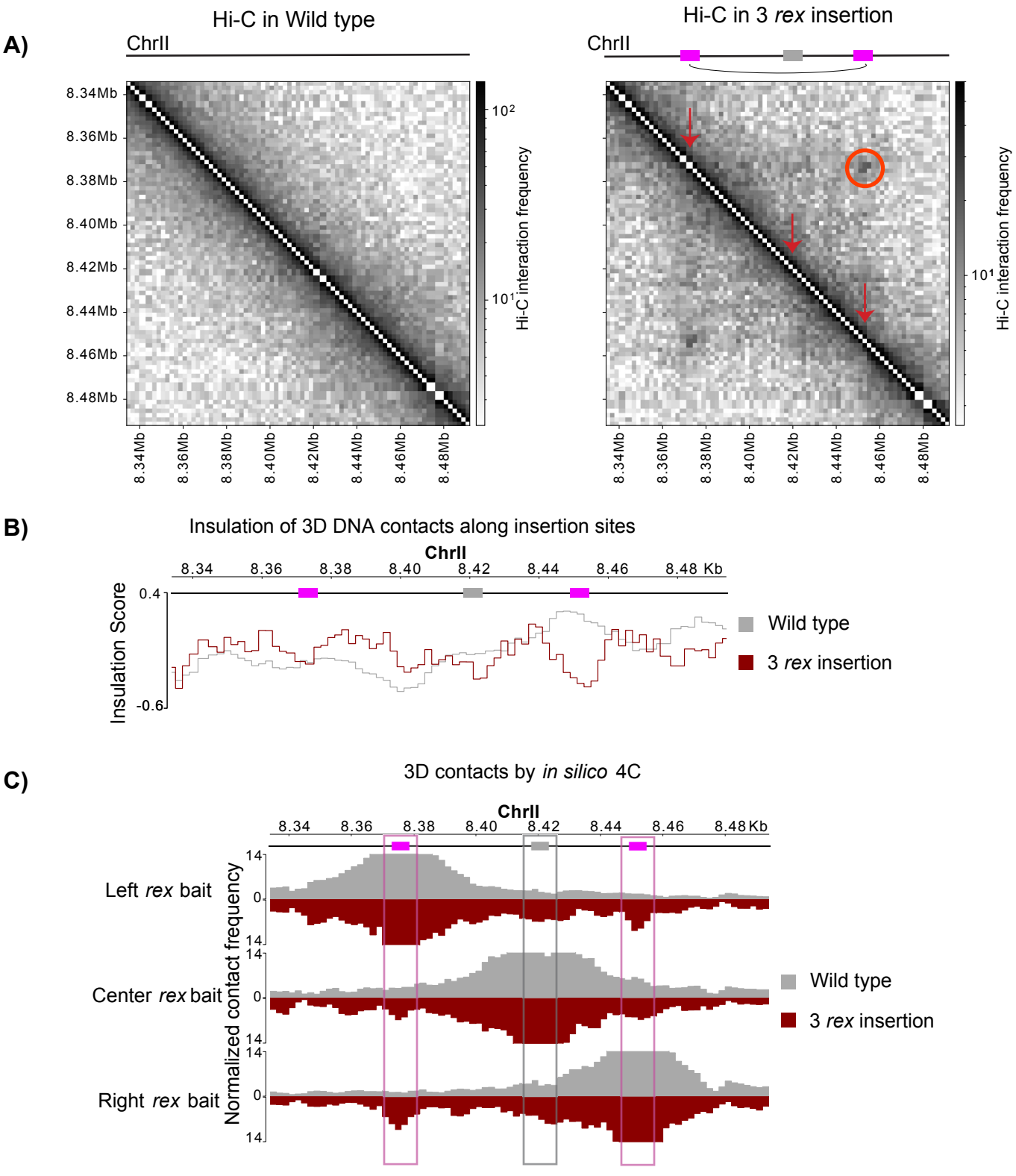
A)
Hi-C in Wild type
ChrII
8.34Mb
8.36Mb
8.38Mb
8.40Mb
8.42Mb
8.44Mb
8.46Mb
8.48Mb
Hi-C interaction frequency
Hi-C in 3 rex insertion
B)
Insulation of 3D DNA contacts along insertion sites
ChrII
8.34 8.36 8.38 8.40 8.42 8.44 8.46 8.48 Kb
Insulation Score
0.4
-0.6
Wild type
3 rex insertion
C)
3D contacts by in silico 4C
ChrII
8.34 8.36 8.38 8.40 8.42 8.44 8.46 8.48 Kb
Left rex bait
Center rex bait
Right rex bait
Normalized contact frequency
Wild type
3 rex insertion

Figure 3

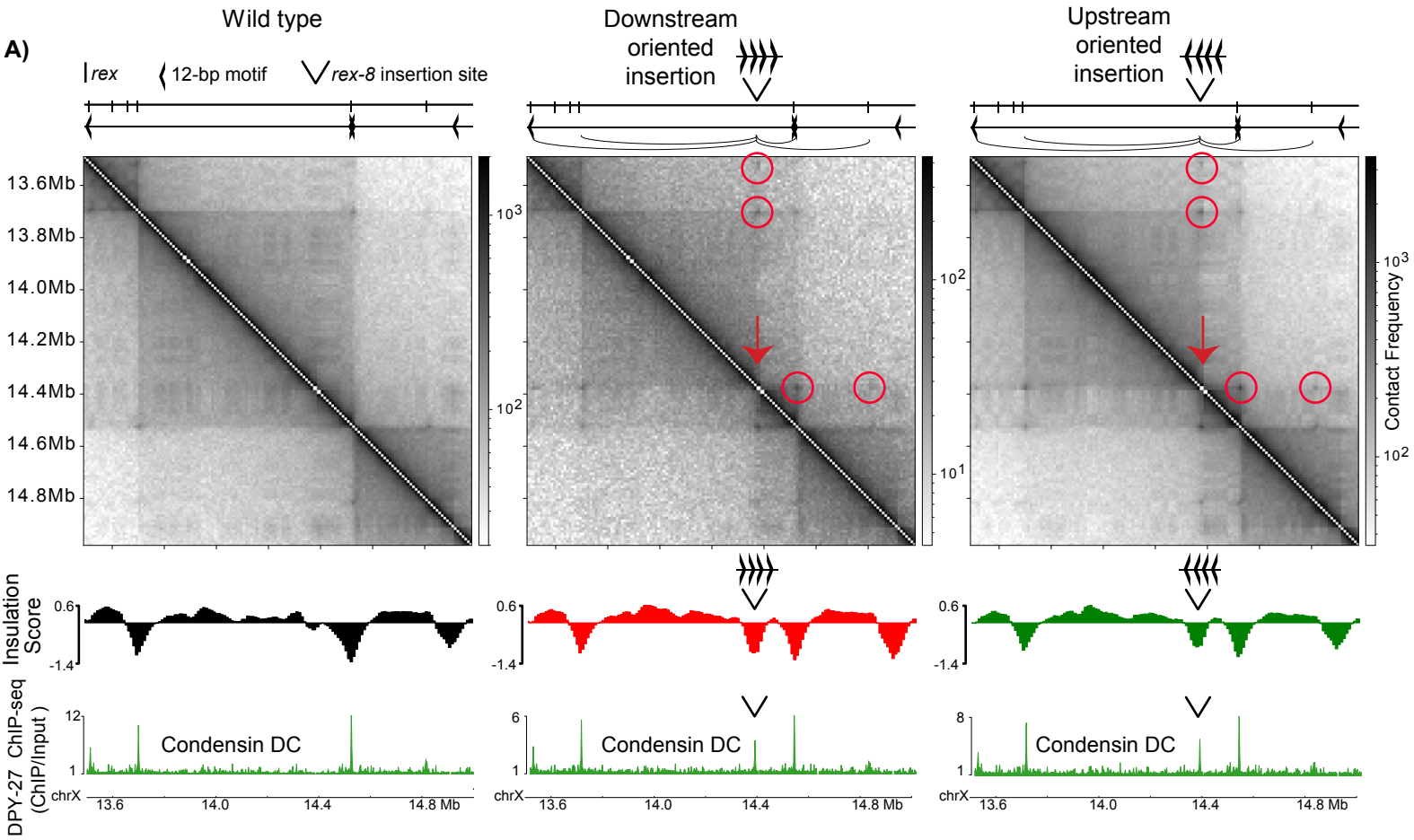
A)
Wild type
rex
12-bp motif
rex-8 insertion site
Downstream oriented insertion
Upstream oriented insertion
13.6Mb
13.8Mb
14.0Mb
14.2Mb
14.4Mb
14.6Mb
14.8Mb
Contact Frequency
Insulation Score
DPY-27 ChIP-seq (ChIP/Input)
Condensin DC
chrX
13.6
14.0
14.4
14.8 Mb

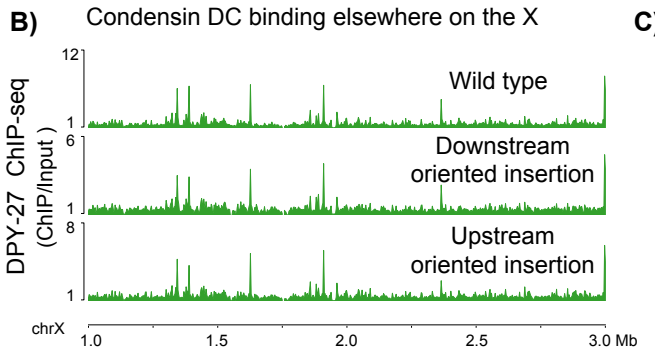
B)
Condensin DC binding elsewhere on the X
DPY-27 ChIP-seq (ChIP/Input)
Wild type
Downstream oriented insertion
Upstream oriented insertion
chrX
1.0
1.5
2.0
2.5
3.0 Mb

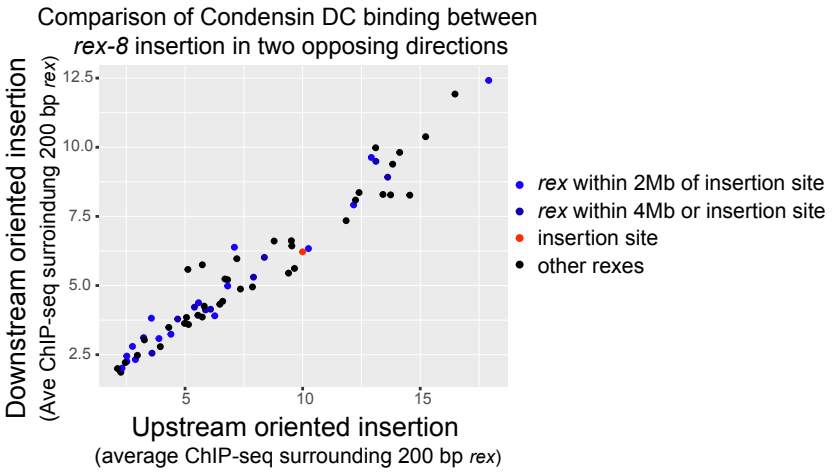
C)
Comparison of Condensin DC binding between rex-8 insertion in two opposing directions
Downstream oriented insertion (Ave ChIP-seq surroindung 200 bp rex)
Upstream oriented insertion (average ChIP-seq surrounding 200 bp rex)
rex within 2Mb of insertion site
rex within 4Mb or insertion site
insertion site
other rexes

Figure 3 Supplement

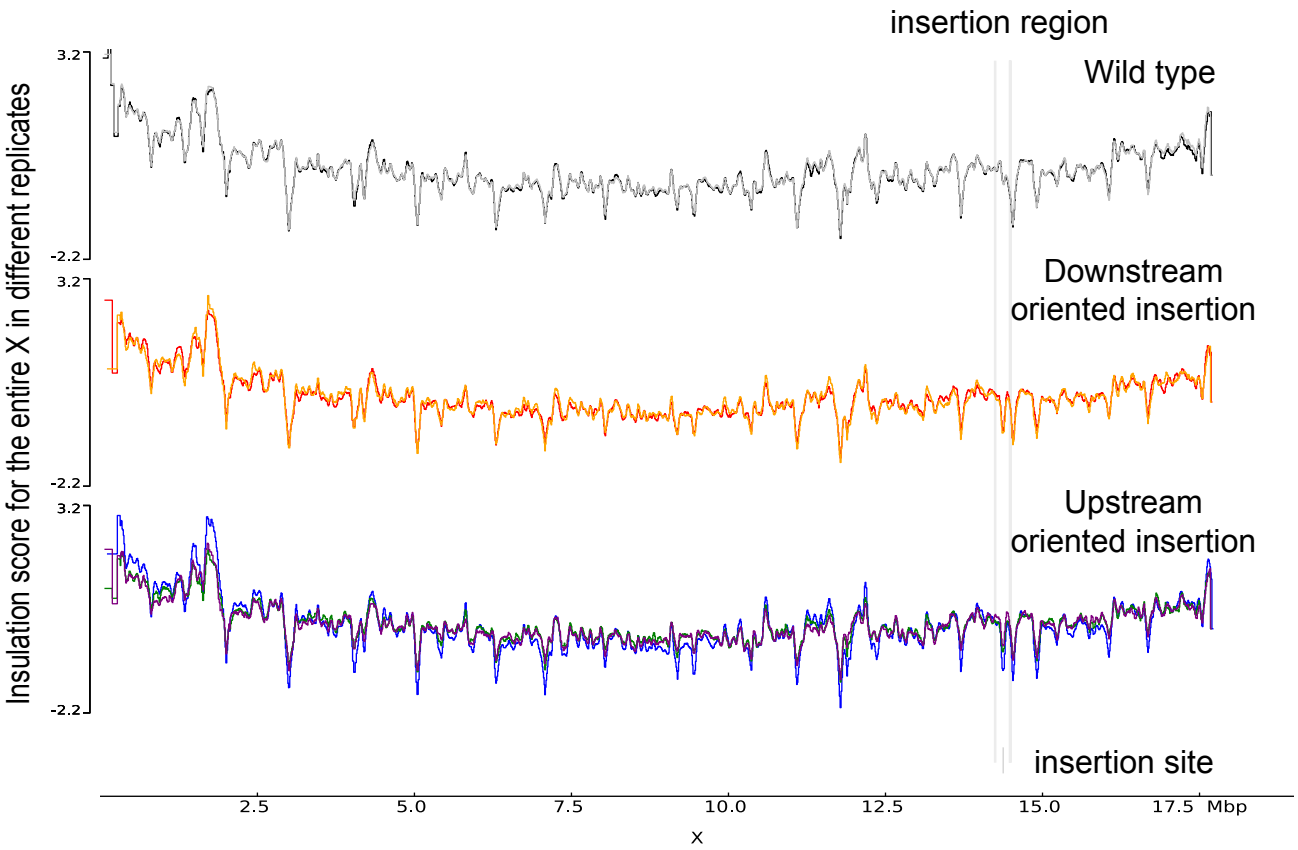

Figure 4

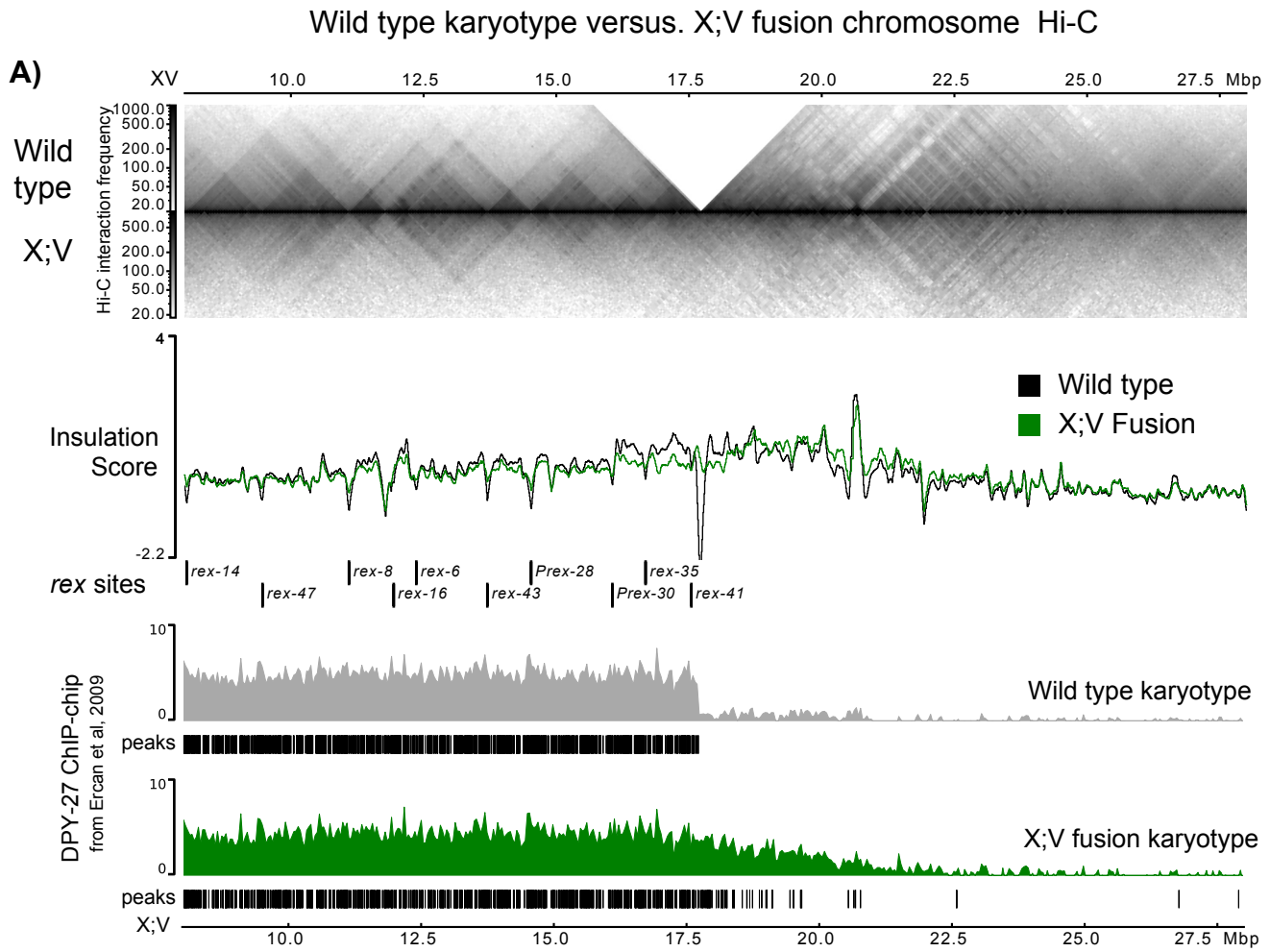
Wild type karyotype versus. X;V fusion chromosome Hi-C
A)
XV
10.0
12.5
15.0
17.5
20.0
22.5
25.0
27.5 Mbp
Wild type
X;V
Hi-C interaction frequency
1000.0
500.0
200.0
100.0
50.0
20.0
Insulation Score
4
-2.2
Wild type
X;V Fusion
rex sites
rex-14
rex-47
rex-8
rex-16
rex-6
rex-43
Prex-28
Prex-30
rex-35
rex-41
DPY-27 ChIP-chip
from Ercan et al, 2009
10
0
Wild type karyotype
peaks
X;V fusion karyotype
X;V

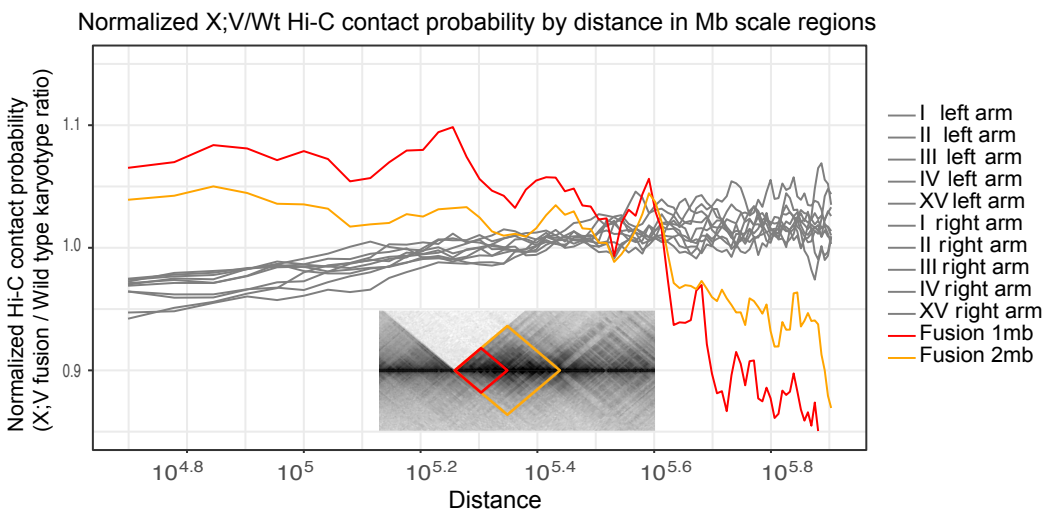
B)
Normalized X;V/Wt Hi-C contact probability by distance in Mb scale regions
Normalized Hi-C contact probability
(X;V fusion / Wild type karyotype ratio)
1.1
1.0
0.9
$10^{4.8}$
10^{5}
$10^{5.2}$
$10^{5.4}$
$10^{5.6}$
$10^{5.8}$
Distance
I left arm
II left arm
III left arm
IV left arm
XV left arm
I right arm
II right arm
III right arm
IV right arm
XV right arm
Fusion 1mb
Fusion 2mb

Figure 4 Supplement

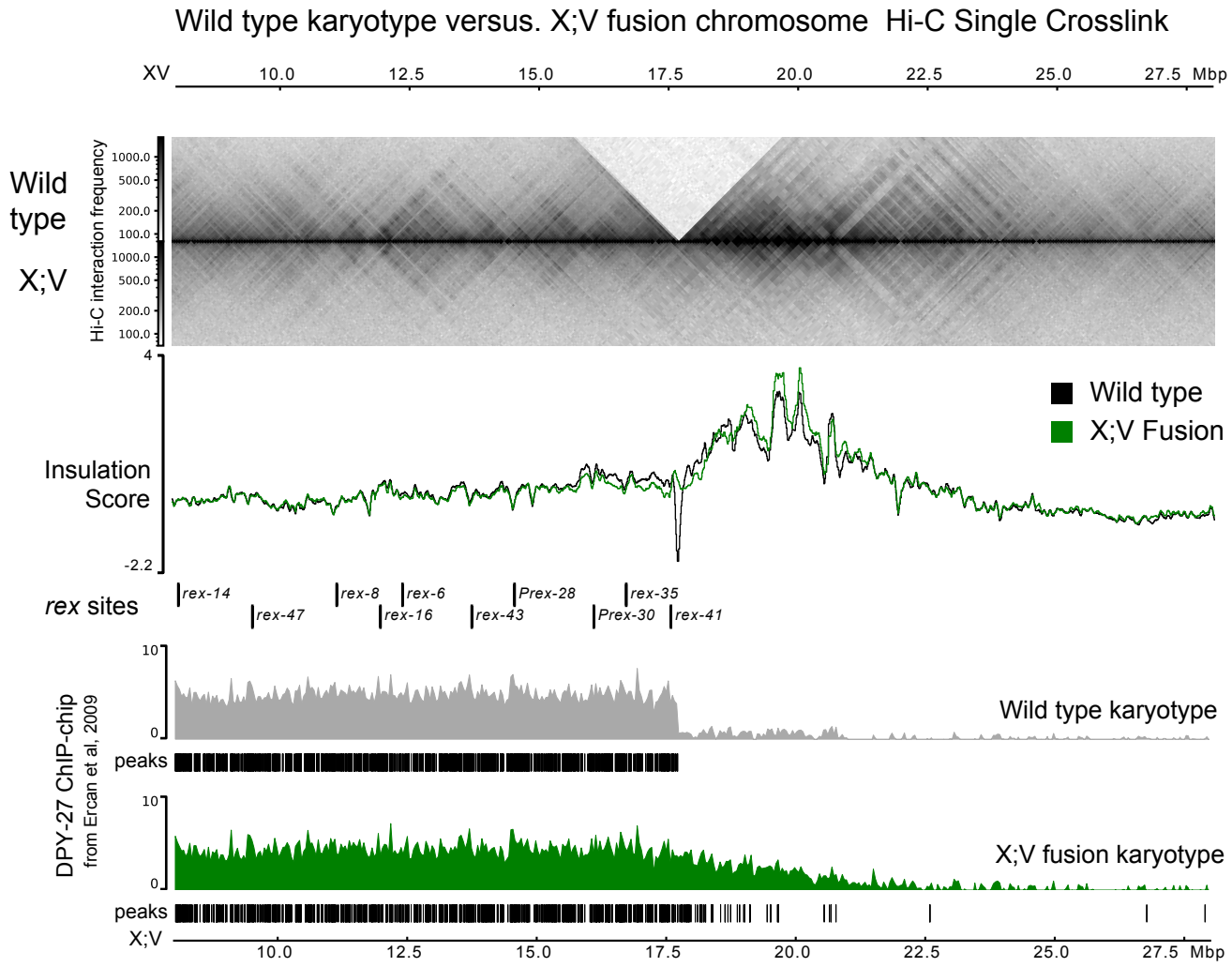

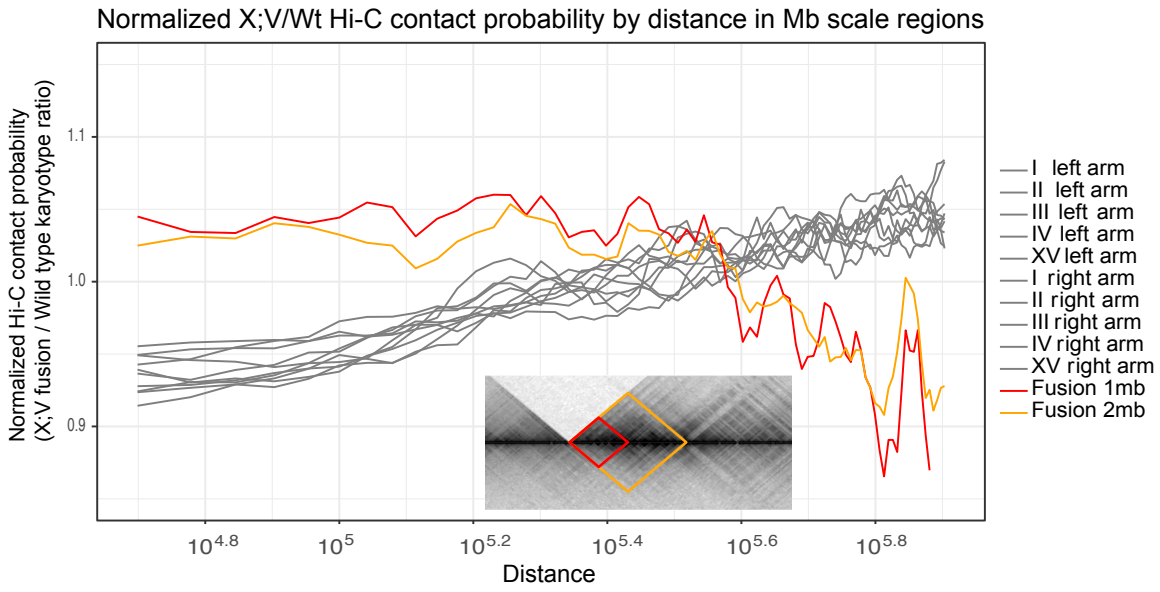

Figure 5

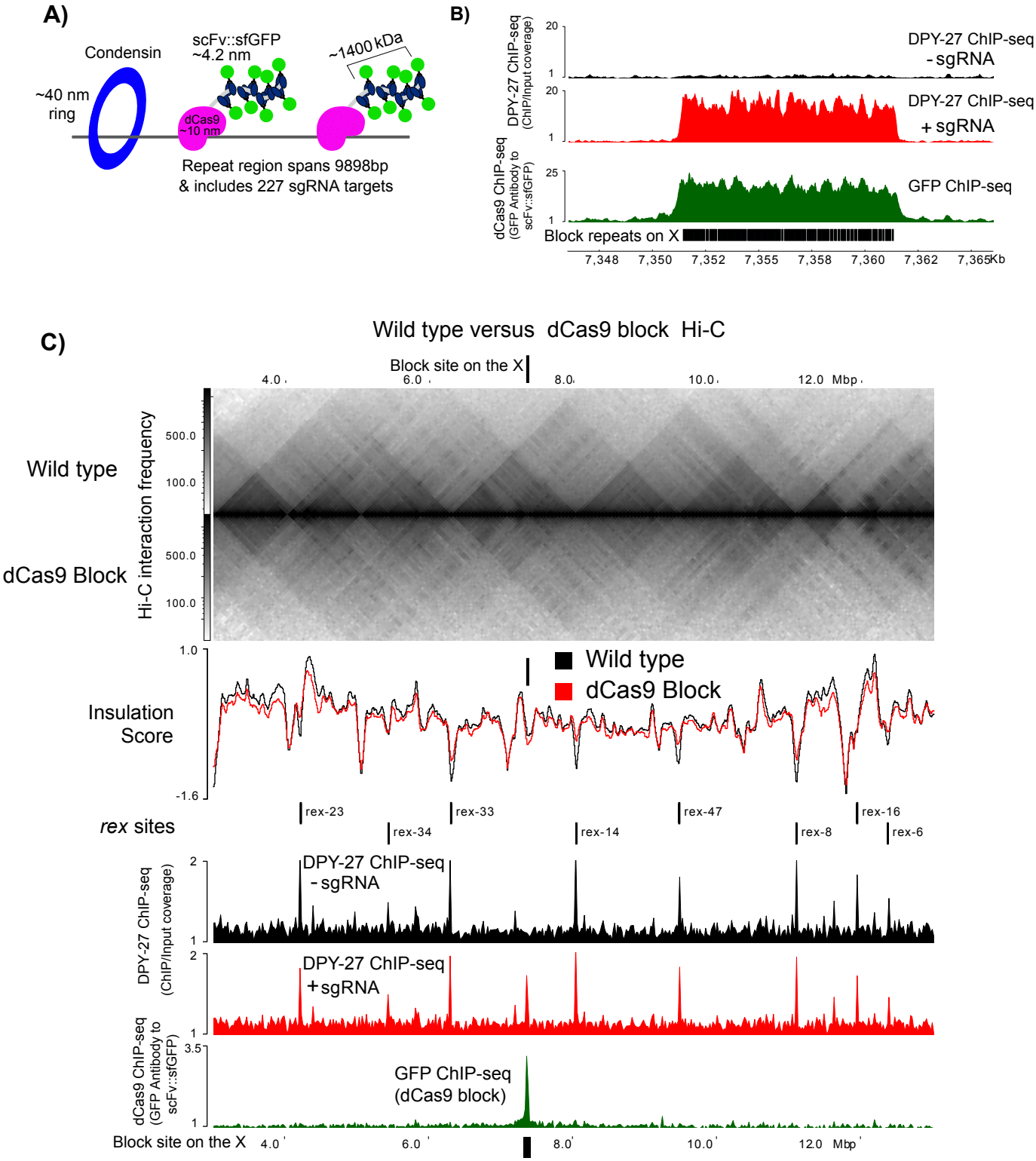
A)
Condensin
~40 nm ring
scFv::sfGFP ~4.2 nm
~1400 kDa
dCas9 ~10 nm
Repeat region spans 9898bp & includes 227 sgRNA targets
B)
DPY-27 ChIP-seq (ChIP/Input coverage)
DPY-27 ChIP-seq - sgRNA
DPY-27 ChIP-seq + sgRNA
dCas9 ChIP-seq (GFP Antibody to scFv::sfGFP)
GFP ChIP-seq
Block repeats on X
7,348 7,350 7,352 7,355 7,358 7,360 7,362 7,365Kb
C)
Wild type versus dCas9 block Hi-C
Block site on the X
4.0 6.0 8.0 10.0 12.0 Mbp
Wild type
dCas9 Block
Hi-C interaction frequency
500.0 100.0 500.0 100.0
Insulation Score
1.0 -1.6
Wild type
dCas9 Block
rex sites
rex-23 rex-33 rex-47 rex-16 rex-34 rex-14 rex-8 rex-6
DPY-27 ChIP-seq - sgRNA
DPY-27 ChIP-seq + sgRNA
GFP ChIP-seq (dCas9 block)
Block site on the X 4.0 6.0 8.0 10.0 12.0 Mbp

Figure 6

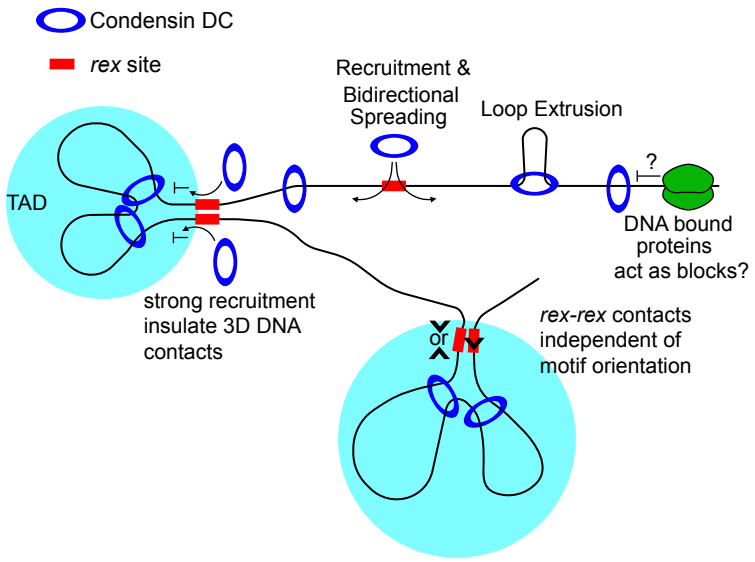
Condensin DC
rex site
Recruitment &
Bidirectional
Spreading
Loop Extrusion
TAD
?
DNA bound
proteins
act as blocks?
strong recruitment
insulate 3D DNA
contacts
or
rex-rex contacts
independent of
motif orientation